# Evaluation of a second order simulation for Sterling engine design and optimisation

**Johannes M Strauss**
*Department of Electrical and Electronic Engineering, Faculty of Engineering, University of Stellenbosch*

**Robert T Dobson**
*Department of Mechanical and Megatronic Engineering Faculty of Engineering, University of Stellenbosch*

***Abstract***
*This paper reports on the investigation of the simulation accuracy of a second order Stirling cycle simulation tool as developed by Urieli (2001) and improvements thereof against the known performance of the GPU-3 Stirling engine. The objective of this investigation is to establish a simulation tool to perform preliminary engine design and optimisation.*

*The second order formulation under investigation simulates the engine based on the ideal adiabatic cycle, and parasitic losses are only accounted for afterwards. This approach differs from third order formulations that simulate the engine in a coupled manner incorporating non-idealities during cyclic simulation. While the second order approach is less accurate, it holds the advantage that the degradation of the ideal performance due to the various losses is more clearly defined and offers insight into improving engine performance. It is therefore particularly suitable for preliminary design of engines.*

*Two methods to calculate the performance and efficiency of the data obtained from the ideal adiabatic cycle and the parasitic losses were applied, namely the method used by Urieli and a proposed alternative method. These two methods differ essentially in how the regenerator and pumping losses are accounted for.*

*The overall accuracy of the simulations, especially using the proposed alternative method to calculate the different operational variables, proved to be satisfactory. Although significant inaccuracies occurred for some of the operational variables, the simulated trends in general followed the measurements and it is concluded that this second order Stirling cycle simulation tool using the proposed alternative method to calculate the different operational variables is suitable for preliminary engine design and optimisation.*

*Keywords: Stirling engines, Second order simulation*

## 1. Introduction

Stirling engine technology has been around for nearly two hundred years, and while these engines have obvious advantages compared to internal combustion engines, they have only recently started to appear as commercialised units. Too date, only a handful of manufacturers have started to produce, or are in the process of commercialising engines based on the Stirling cycle.

Many difficulties encountered in the past that are either unique or critical to the functioning of Stirling engines have contributed to its slow development. These include, amongst others, adequate and uniform heat transfer at high temperature to the working gas, lubrication of the pistons, seals and sealing, and regenerator contamination. Critical to the establishment of the Stirling engine, some of these difficulties could not be resolved at the time, while giant strides were made with the internal combustion engine to become the engine of the future (Hargreaves, 1991).

During the past few decades, as technology and materials improved, these difficulties were largely resolved and today Stirling engines are preferred in certain niche applications due to a few unique advantages, including low noise operation, long-term operational capabilities and efficiency. These advantages make the Stirling engine a strong contender for the conversion of heat energy to electrical energy using various heat sources, including fossil and renewable fuels, solar heat and waste heat.

In this regard, research on the per cycle simulation of the thermodynamic and gas dynamic behaviour of Stirling engines has helped to improve our understanding of these processes and helped with optimization of engines.

Stirling cycle analysis has been approached in a variety of ways. With the focus here being cyclic thermodynamic and gas dynamic behaviour, one such approach (broadly known as nodal or finite-cell analysis) strives to obtain numerical solutions to the various thermodynamic variables, e.g. temperature and pressure, as a function of location and time throughout the engine. This method falls within the range of methods commonly referred to in Stirling cycle analysis as second order or third order simulation, depending on the complexity with which the simulation is approached (Organ, 1992).

Nodal analysis or finite-cell analysis entails the subdivision of the flow passages, i.e. the heat exchangers and regenerator, into a number of cells and the subsequent formulation of the engineering form of the conservation equations for these cells in terms of finite differences. The variable volumes of the expansion and compression spaces are described by an adiabatic model. The momentum and energy equations may be simplified by omitting some of the terms. An energy balance for the walls of the flow passages may or may not be part of the formulation. This analysis is attractive in that sufficient detail is generated to form a picture of gas pressures, mass flow, gas and metal temperatures and so forth as a function of location and time (Organ, 1992).

Probably the most influential of these formulations include those of Urieli and Berchowitz. Urieli (1977) developed a one-dimensional approach with complete differential equations of continuity, momentum and energy of the working gas and energy of the regenerator matrix and heat exchanger walls. In addition, kinetic energy terms are included in the energy equation of the working gas, while gas acceleration effects are included in the momentum equation.

Berchowitz (1978) continued to improve on the work of Urieli, e.g. by including viscous dissipation in the working gas. Berchowitz also identified errors and unnecessary assumptions in the formulation of Urieli and proposed corrections thereof. These are truly third order formulations and are particularly suitable to investigate different engine configurations and working conditions, with the further advantage of being able to observe the thermodynamic and gas dynamic behaviour of the engine at any given time or location.

While the forementioned formulations approach the engine simulation in a coupled fashion, i.e. all of the loss mechanisms are included in the cyclic thermodynamic simulation of the engine, simplified decoupled analysis, also known as second order analysis, simulates the engine based on the ideal adiabatic cycle and parasitic losses are only accounted for afterwards. While this approach is less accurate, it holds the advantage that the degradation of the ideal performance due to the various losses is better identified and thus offers insight for improving engine performance. This method is therefore particularly suitable for preliminary design of engines (Berchowitz, 1986).

Berchowitz (1986) went on to develop a second order approach with preliminary design and optimisation as its objective. This method was then used to test its accuracy against three well documented Stirling engines of which the GPU-3 (Ground Power Unit), a rhombic drive Stirling engine generator set developed by the General Motor Research Laboratories, is probably the best documented Stirling engine available to the public.

Urieli and Berchowitz (1984) developed a simplified variation of this approach that later served as a basis for a course that Urieli (2001) presented at the Ohio University in Athens, Ohio, on Stirling cycle machine analysis, where the machine analysis was also implemented by Urieli in the mathematical software package MATLAB.

In a recent investigation, Snyman *et al.* (2008) simulated a Heinrici Stirling engine with this simplified variation and compared the simulated results with experimental data. The simulation was found to be fairly accurate. The Heinrici Stirling engine is, however, not a high performance engine, i.e. it consists of only three main volumes, namely an integrated expansion space/hot side heat exchanger and compression space/cold side heat exchanger with a flow passage in between, also acting as a very inefficient regenerator. In modern high performance engines, with highly efficient regenerators, the expansion space/hot side heat exchanger and compression space/cold side heat exchanger respectively are separate volumes to improve heat transfer, yielding a five volume topology. The question still remains then to what extent this simplified variation, developed by Urieli and Berchowitz (1984), is capable of accurately simulating high performance Stirling engines.

In this paper, implementation of this simplified variation as developed by Urieli (2001) in the open source scripting language Python and the verification of its simulation accuracy against the known performance of the GPU-3 Stirling engine, are reported. The objective of this investigation is to establish a simulation tool to perform preliminary engine design and optimization and forms part of a longer term Stirling engine research effort at the University of Stellenbosch.

## 2. Ideal adiabatic numerical formulation

Consider the alpha type engine configuration in Figure 1 indicating the simulation variables for the

ideal adiabatic approach. In Figure 1, $W$, $V$, $m$, $T$, $Q$ and $p$ refer to work, volume, mass, temperature, heat and pressure respectively. The subscripts $c$, $k$, $r$, $h$, and $e$ refer to the compression space, cooler or cold side heat exchanger, regenerator, heater or hot side heat exchanger and expansion space respectively. The double subscripts $ck$, $kr$, $rh$, and $he$ refer to the four interfaces between the respective cells.

The engine is subdivided into five cells, corresponding to the compression, cooler, regenerator, heater and expansion spaces respectively. The compression and expansion spaces are considered to be adiabatic. Energy is transferred across the interfaces between the cells by means of enthalpy transferred to and from the working spaces in terms of mass flow and upstream temperature. The cooler and heater act as an ideal energy sink and source respectively, i.e. the temperature of the working gas in the heat exchangers is considered to be equal to the heater and cooler temperatures. Regeneration is considered to be ideal.

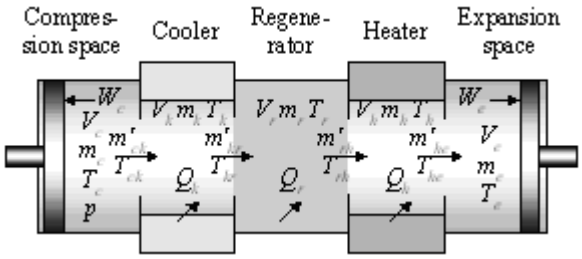


**Figure 1: Diagram of alpha type engine showing simulation variables**
*Source: Urieli, 2001*

Figure 2 shows the temperature profile of the ideal adiabatic approach. It is shown that the temperature of the flow passages, that is the cooler, regenerator and heater, is fixed, with only the variable volume temperatures that change due to the assumption that the processes are adiabatic.

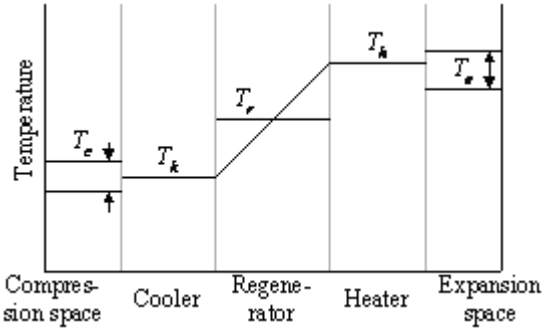


**Figure 2: Temperature profile of the ideal adiabatic approach**
*Source: Urieli, 2001*

With reference to Figure 3 showing a generalised cell, governing equations for the adiabatic model are derived from the energy equation (Urieli, 2001)

$$dQ + (c_p T_i m'_i - c_p T_o m'_o) = dW + c_v d(mT), \quad (1)$$

the equation of state

$$pV + mRT, \quad (2)$$

and the equation of state in differential form (Urieli, 2001)

$$dp/p + dV/V = dm/m + dT/T, \quad (3)$$

for each of the five cells, where $c_p$ and $c_v$ refer to the specific heat capacities of the gas at constant pressure and constant volume respectively. The subscripts $i$ and $o$ refer to inflowing and outflowing respectively and $m'$ denotes the rate of mass flow. The law of conservation of mass is used to link the resulting equations.

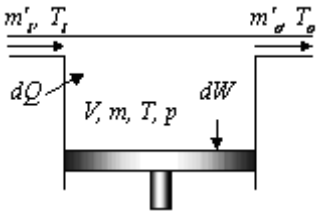


**Figure 3: Generalised cell**
*Source: Urieli, 2001*

The complete set of equations describing the ideal adiabatic simulation of the five cell engine as shown above is given in Appendix A. It is found that there are twenty-two variables and sixteen derivatives to be solved for a single cycle. The variables can be divided as follows (Urieli, 2001):

- Seven variables of which the derivatives need to be integrated: $T_c$, $T_e$, $Q_k$, $Q_r$, $Q_h$, $W_e$, $W_c$.
- Nine analytical variables and derivatives: $W$, $p$, $V_e$, $V_c$, $m_c$, $m_k$, $m_r$, $m_h$, $m_e$.
- Six conditional and mass flow variables: $T_{ck}$, $T_{he}$, $m'_{ck}$, $m'_{kr}$, $m'_{rh}$, $m'_{he}$.

Quasi-steady flow is assumed, which implies that the four mass flow variables remain constant over each integration interval with no acceleration effects. The problem thus reduces to the simultaneous solution of a set of seven ordinary differential equations.

The simplest approach to solve this set of ordinary differential equations is to formulate it as an initial-value problem, where the initial values of all the variables are known and the equations are integrated from this initial state over a complete cycle, i.e. where the crank completes one full rotation (360 degrees) bringing the pistons back to their initial positions. It should be noted that the ideal adia-

batic model is not an initial-value problem, but rather a boundary-value problem, since we do not know the various initial values. However, by assigning arbitrary initial conditions for the seven variables to be integrated and integrating the equations through several complete cycles, the cyclic steady state can be attained where the respective values at the beginning of the cycle and at the end of the cycle are equal. According to Urieli (2001), the most sensitive measure of convergence to a cyclic steady state is the residual regenerator heat $Q_r$ at the end of the cycle, which should be zero.

## 3. Expanded second order numerical formulation

Urieli and Berchowitz (1984) further expanded their second order formulation to consider non-ideal effects including non-ideal regeneration, non-ideal heat exchangers, heat leakage of the regenerator wall and pumping losses. The first two loss mechanisms may be illustrated as follows in the temperature profile of Figure 4.

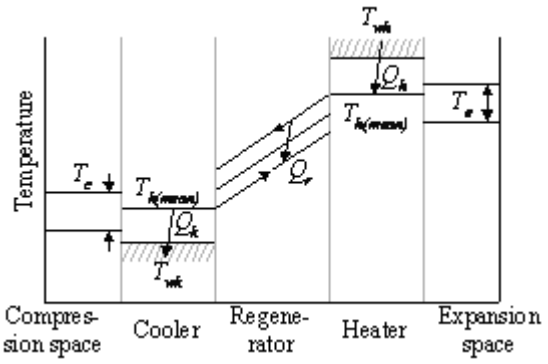


**Figure 4: Temperature profile for non-ideal regeneration and heat exchangers**
*Source: Urieli, 2001*

In Figure 4, the subscripts *wh* and *wk* refer to the heater wall and cooler wall respectively. The temperature profile of Figure 4 differs from that of Figure 2 by allowing for non-ideal regeneration and non-ideal heat exchanging.

### *Non-ideal heat exchangers*

Non-ideal heat exchanging will result in the mean cooler and heater gas temperatures that differ from that of the exchanger walls.

From the basic equation for convective heat transfer we obtain

$$\dot{Q} = hA_{wg}\left(T_w - T\right), \tag{4}$$

where $\dot{Q}$ is the tempo of heat transferred, $h$ is the convective heat transfer coefficient, $A_{wg}$ refers to the wall or wetted area of the heat exchanger surface, $T_w$ is the wall temperature and $T$ is the gas temperature.

While ideal heat exchanging was assumed for the ideal adiabatic formulation, resulting in no difference between the gas temperatures and the wall temperatures, non-ideal heat exchanging is now taken into account. From (4), with $h$ having a finite value, the gas temperatures in the heat exchangers and the heat exchanger wall temperatures will now differ.

The per cycle heat transferred for the cooler and the heater is thus

$$Q_k = h_k A_{wgk}(T_{wk} - T_{k(mean)}/f \tag{5}$$

and

$$Q_k = h_h A_{wgh}(T_{wh} - T_{h(mean)}/f \tag{6}$$

respectively, where $f$ denotes the rotational frequency in cycles per second.

### *Non-ideal regeneration*

Regeneration was assumed to be perfect in the ideal adiabatic approach. By definition, a regenerator is a cyclic device. During the first part of the cycle, referred to as a "single blow", the hot gas flows through the regenerator from the heater to the cooler and heat is transferred to the regenerator matrix. During the second part of the cycle, the cold gas flows in the reverse direction and heat is absorbed that was previously stored in the matrix. Urieli (2001) proposed the following definition of regenerator effectiveness $\varepsilon$ as

$$\varepsilon = \frac{\text{amount of heat transferred from matrix to gas during a single blow through thegenerator}}{\text{equivalent amount of heat transferred in the regenerator of the ideal adiabatic model}} \tag{7}$$

Regenerator effectiveness varies from 1 for an ideal regenerator to 0 for no regenerative action. For non-ideal regeneration in a system with the gas flowing from the cooler to the heater during a single blow, the gas will have a temperature somewhat lower than that of the heater on exit from the regenerator. This will result in more heat being supplied externally over the cycle by the heater in increasing the temperature of the gas to that of the heater and can be written quantitatively as

$$Q_h = Q_{hi} + \hat{Q}_{ri}\left(1 - \varepsilon\right), \tag{8}$$

where $Q_h$ and $Q_{hi}$ refer to the net heat transferred to the working gas in the heater for the non-ideal case and ideal adiabatic case respectively and $\hat{Q}_{ri}$ refers to the amount of heat transferred during a single blow to or from the regenerator for the ideal adiabatic case. $\hat{Q}_{ri}$ may therefore refer to the amount of

heat transferred to the regenerator for the single blow when the working gas flows from the heater to the cooler. Alternatively, it may refer to the amount of heat transferred from the regenerator for the single blow when the working gas flows from the cooler to the heater. The enthalpy loss of the regenerator is therefore identified from equation (8) as

$$Q_{rloss} = \hat{Q}_{ri}(1-\varepsilon). \quad (9)$$

The regenerator effectiveness $\varepsilon$ can be determined from the Number of Transfer Units (NTU), which is a well known measure of heat exchanger effectiveness by

$$\varepsilon = \frac{\text{NTU}}{1 + \text{NTU}.} \quad (10)$$

The NTU values can be obtained in terms of the Stanton number by

$$NTU = N_{ST}(A_{wg}/A)/2. \quad (11)$$

The Stanton number is obtained in turn from the average Reynolds number determined over one cycle.

***Regenerator wall heat leakage***

Regenerator wall heat leakage, due to heat flow from the heater to the cooler via the walls of the regenerator, is determined from

$$Q_{rwl} = C_{qwr}(T_{wh} - T_{wk})/f, \quad (12)$$

where $Q_{rwl}$, $C_{qwr}$, $T_{wh}$, $T_{wk}$ and $f$ denote the heat loss per cycle due to wall heat leakage, regenerator housing thermal conductance, heater wall temperature, cooler wall temperature and operating frequency respectively.

***Pumping work loss***

While pressure was assumed to be constant throughout the engine, fluid friction associated with the flow through the heat exchangers and the regenerator will in fact result in a pressure drop between the variable volumes. This reduces the power output of the engine and is known as pumping work losses. Pressure drop is evaluated from

$$\Delta p = \frac{-2C_{ref}\mu u V}{d_h^2 A}, \quad (13)$$

for each of the heat exchangers and the regenerator. The Reynolds friction coefficient $C_{ref}$ is calculated from the Reynolds number for the specific fluid conditions at a given time for specific heat exchanger and regenerator topologies. In (13), $\mu$, $u$, $V$, $d_h$, and $A$ denote the working gas dynamic viscosity, the fluid mean bulk velocity, the void volume, the hydraulic diameter and the internal free flow area respectively.

The pressure drop is evaluated for each of the heat exchangers and the regenerator for the entire cycle. The pressure drop for the three volumes is summated at each point for the entire cycle and is added to the compression space pressure to obtain a new expansion space pressure. The pumping loss per cycle is then calculated by integration of the product of pressure drop and the derivative of the variable expansion space volume for one cycle as follows, namely

$$\Delta W = \int_0^{2\pi} \left( \sum_{i=1}^{3} \Delta p_i \frac{dV_e}{d\theta} \right) d\theta, \quad (14)$$

where $\Delta p_i$ denotes the total pressure drop across the heater, regenerator and cooler and $dV_e$ denotes the derivative of the variable expansion space volume.

***Second order formulation simulation flow***

The second order numerical formulation discussed here was implemented in the open source scripting language Python. Figure 5 shows a block diagram representation of the simulation flow. In Figure 5, the subscripts *gh* and *gk* denote the heater and cooler gas temperatures respectively. The two variables $T_{gh}$ and $T_{gk}$ are therefore equivalent to $T_h$ and $T_k$ and are used to calculate iteratively new gas temperatures as shown in Figure 5 (on next page).

During initialisation, the heater and cooler wall temperatures $T_{wh}$ and $T_{wk}$ are set equal to the input heater and cooler temperatures $T_h$ and $T_k$ respectively.

The simulation then iteratively determines the temperature of the gas in the heater and cooler, $T_{gh}$ and $T_{gk}$ respectively, as was explained previously. This is done by first performing an ideal adiabatic simulation, followed by a calculation of the new gas temperatures according to the information received from the ideal adiabatic simulation. The regenerator enthalpy and heat leakage losses and the pumping work loss are determined once convergence is obtained, i.e. when the newly determined gas temperatures and the gas temperatures determined during the previous iteration are within a certain tolerance.

Two different methods exist to calculate the performance and efficiency of the engine after the simulation is completed. These two methods are explained with the help of heat/work flow diagrams as shown in Figure 6.

In Figure 6, $q_{in\_total}$ denotes the total input heat to the engine, $q_{r\_enthalpy}$ and $q_{r\_wall}$ denote the regenerator enthalpy and wall heat leakage losses respectively, $q_{heat}$ and $q_{cool}$ denote the heat input to and heat rejected from the gas cycle respectively, $q_{out\_total}$ denotes the total heat rejected at the cooler, $w_{pumping}$ denotes pumping work loss and $w_{result}$ denotes the resultant output work.

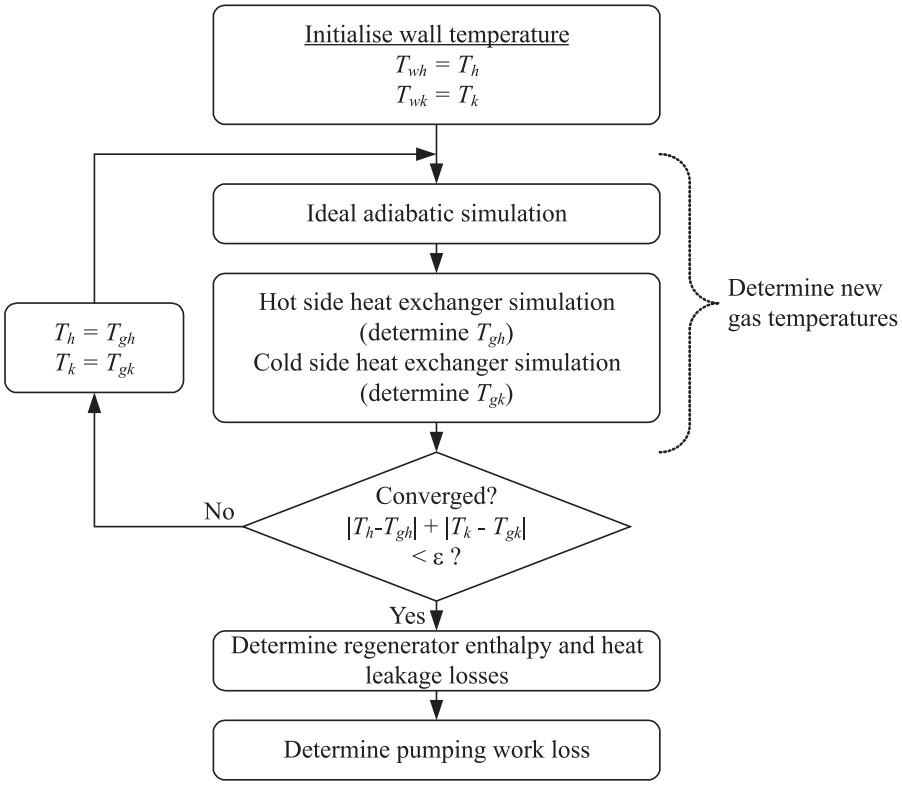


**Figure 5: Second order simulation flow**
*Source: Urieli, 2001*

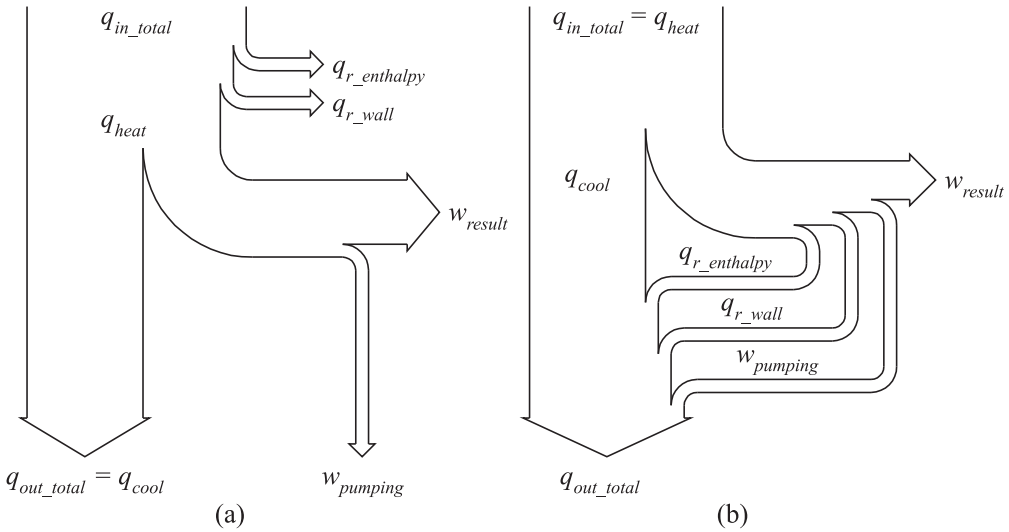


**Figure 6: Heat and work flow diagrams for performance and efficiency calculations**

The first diagram shown in Figure 6a represents the method used by Urieli (2001) to calculate the performance and efficiency of the engine and will be called the Urieli method. The second method shown in Figure 6b represents an alternative calculation of the performance and efficiency and will be denoted the alternative method.

The difference between the two methods is essentially how the regenerator and pumping losses are accounted for. In the case of the Urieli method, these losses are added to the simulated heat input of the cycle to obtain a new total heat input to the engine. Urieli did not explain his decision to calculate engine performance in this manner. In practice, his approach means that the heater temperature will have to be set higher to achieve the higher heat input to the engine, effectively changing the original simulation input parameters.

The alternative method tries to avoid this by subtracting the regenerator losses from the simulat-

ed output work and adding these losses to the heat rejected from the gas to obtain a new total amount of heat that is rejected from the cooler. The reasoning for this alternative is that the regenerator losses calculated after the cyclic simulation will in practice degrade the engine by lowering the output power and by increasing the rejected heat at the cooler. As a result, gas cycle variables for the more realistic simulation will inevitably differ from that obtained during cyclic simulation, e.g. the maximum and minimum pressure values will decrease and increase respectively. This should be kept in mind when interpreting and using gas cycle variables obtained during cyclic simulation.

As for the pumping losses, it was realised that heat generated due to gas friction will also have to be rejected at the cooler. However, not all heat generated per cycle due to gas friction will be rejected. In following Berchowitz (1986), only half of the heat generated in the regenerator and the heat generated in the cooler due to gas friction is considered as lost. The remaining heat generated in the regenerator and the heat generated in the heater remains a useful part of the thermodynamic cycle. The quantity, $w_{pumping}$, as shown in Figure 6b, therefore only accounts for the gas friction losses or pumping losses rejected at the cooler.

It follows that the total input heat to the engine is more for the Urieli method, the resultant output work is less and the total output heat is more for the alternative method. In section 5, both these methods will be compared to the experimental results obtained by Thieme (1979, 1981).

## 4. Simulation of the GPU-3 Stirling engine

The GPU-3 Stirling engine was originally built by General Motors Research Laboratories for the U.S. Army in 1965, as part of a 3 kWe engine-generator set that was designated the Ground Power Unit 3. This is a single cylinder, displacer engine (beta configuration) with a rhombic drive and power output of up to approximately 9 kWe with hydrogen as working fluid at 6.9 MPa average pressure and 3 600 rpm rotational speed (Thieme, 1979).

The GPU-3 specifications were well documented by Thieme (1979, 1981) and later by Organ (1992, 1997) and are listed in Appendix B.

According to the data provided in Appendix B, the heat exchangers have sections that are not exposed to the heat or to the coolant and should therefore be considered only contributing to the overall void volume. The second order formulation presented here does not specifically provide for such inactive void volumes in the heat exchangers. Since these volumes cannot be ignored it was decided to approximate the GPU-3 implementation by adding the void volumes in the heat exchangers to the void volumes of the adjacent volumes. The clearance distances of the pistons in the expansion and compression spaces were therefore increased to account for the heat exchanger volumes adjacent to the expansion and compression spaces not exposed to heat or coolant. The calculated void volume of the regenerator was also increased to account for the inactive void volumes of both heat exchangers adjacent to the regenerator.

In most cases, when providing Stirling engine performance data, the average pressure for a certain operating condition is provided. This implies a certain working fluid mass. The second order formulation presented here, however, uses working fluid mass to calculate the pressure and not vice versa. To overcome this problem, where the average pressure is given and the total mass of the gas is unknown, the mass of gas is guessed to start with and is then continually recalculated for each iteration to achieve the given average pressure. All other data that depends on the mass of gas is scaled accordingly.

Of the numerous tests that were conducted, Thieme (1979, 1981) documented one measurement each in detail in the two reports prepared for the U.S. Department of Energy. Table 1 lists the operational information of these two measurements.

**Table 1: Core information of the documented low power baseline and high power baseline measurements conducted by Thieme (1979, 1981)**

| | *Low power baseline* | *High power baseline* |
|---|---|---|
| Working fluid | Helium | Hydrogen |
| Heater-tube gas temp. | 697 °C | 677 °C |
| Mean compression space pressure | 4.13 MPa | 6.92 MPa |
| Engine speed | 2503 rpm | 1504 rpm |

Sullivan (1989) also listed some measured data for the tests that were conducted at the NASA Glenn Research Centre by Thieme. It is against these documented experimental results that the simulation accuracy of the second order formulation is compared.

## 5. Results

Table 2 compares the measured low power baseline measurement documented by Thieme (1979) and the simulated results thereof using the second order formulation described previously.

The second order formulation could predict the average expansion space and compression space temperatures fairly accurately. It should be highlighted though that it is difficult to measure the temperature of the gas in the variable spaces accurately.

**Table 2: Comparison of the measured and simulated low power baseline measurement by Thieme (1979)**

| | *Measured results* | *Simulated results with % error* | |
|---|---|---|---|
| | | *Urieli method* | *Alternative method* |
| Exp. space average temperature | 851 K | 878 K (3.2%) | |
| Comp. space average temperature | 371 K | 350 K (-5.7%) | |
| Exp. space pressure swing | 2.89 MPa | 3.16 MPa (9.3%) | |
| Comp. space pressure swing | 2.94 MPa | 3.01 MPa (2.4%) | |
| Heat input to working fluid per cycle | 272 J | 313 J (15.1%) | 273 J (0.4%) |
| Heat out of working fluid per cycle | 177 J | 115 J (-53.9%) | 165 J (-6.78%) |
| Indicated output power and efficiency | 3.7 kW @ 0.303 | 5.61 kW @ 0.43 (51.6%) | 4.39 kW @ 0.386 (18.6%) |
| Brake output power and efficiency | 2.65 kW @ 0.217 | 4.56 kW @ 0.35 (72.1%) | 3.34 kW @ 0.294 (26.0%) |

The heat input to the engine is over-estimated by the Urieli method. Sullivan (1989) obtained similar results, i.e. of the order of 20%. The alternative method, however, over-estimated the heat input by only 0.4%.

It was expected for the Urieli method to underestimate the heat rejected at the cooler, since the simulation does not take into account during the cyclic simulation the additional heat that should be rejected at the cooler due to the regenerator losses, appendix gap losses, and so forth. The alternative method again predicted the rejected heat more accurately, since at least part of the additional heat is taken into account.

Overestimation of the pressure swing was again expected. It is difficult to attribute one single reason to this inaccuracy due to the interrelated nature of the different loss mechanisms on the gas cycle. However, since the second order formulation described here does not take a variety of losses into account during cyclic simulation that will inevitably degrade the performance of the engine, it should be expected that the pressure-volume work and therefore the pressure swing be overestimated.

The brake output power of the GPU-3, i.e. the output power at the shaft of the engine, was determined by Thieme (1979) to be 2.65 kW as given in Table 2. Thieme (1979, 1981) also determined by experiments and calculations the mechanical losses for the conditions given in Table 2 at 1.05 kW. For comparative purposes, the simulated output power is compared with the measured output power both without (indicated power) and with (brake power) consideration of mechanical losses.

The inaccuracies for the Urieli method should not come as a surprise when considering that the input heat and the heat rejected at the cooler is overestimated and underestimated by approximately 15% and 54% respectively, resulting in the overestimation of the output power. Furthermore, even

**Table 3: Comparison of the measured and simulated high power baseline measurement by Thieme (1981)**

| | *Measured results* | *Simulated results with % error* | |
|---|---|---|---|
| | | *Urieli method* | *Alternative method* |
| Exp. space average temperature | 847 K | 887 K (4.7%) | |
| Comp. space average temperature | 345 K | 335 K (-2.9%) | |
| Exp. space pressure swing | 4.23 MPa | 4.81 MPa (13.7%) | |
| Comp. space pressure swing | 4.43 MPa | 4.77 MPa (7.7%) | |
| Heat input to gas per cycle | 444 J | 507 J (14.2%) | 432 J (-2.7%) |
| Heat out of working fluid per cycle | 245 J | 170 J (-30.6%) | 248 J (1.2%) |
| Indicated output power and efficiency | 4.91 kW @ 0.406 | 6.29 kW @ 0.494 (28.1%) | 4.47 kW @ 0.413 (-9.0%) |
| Brake output power and efficiency | 4.16 kW @ 0.344 | 5.54 kW @ 0.435 (33.2%) | 3.72 kW @ 0.344 (-10.6%) |

if all of the losses were taken into consideration, the simulated output power would still exceed the actual value. This issue was partly addressed for the alternative method, yielding better results.

Table 3 compares the measured high power baseline measurement documented by Thieme (1981) and the simulated results thereof using the second order formulation.

The inaccuracies of the expansion and compression space average temperatures are again satisfactory. The inaccuracies of the simulated expansion space and compression space pressure swings are slightly less accurate in comparison with the low power baseline measurement listed in Table 2.

The heat input to the engine and heat rejected at the cooler were estimated with inaccuracies that are similar to those listed in Table 2, with the exception of the heat rejected calculated with the Urieli method, which improved in accuracy. The accuracy of the output power and efficiency calculated using the Urieli method show a vast improvement, but worsened using the alternative method, when compared to the results listed in Table 2.

In general, the accuracy of the results obtained using the Urieli method improved, but accuracy worsened when using the alternative method. Sullivan (1989) in his investigation reported that the absolute prediction error of the power was greater for helium than for hydrogen. This is also the case using the Urieli method, where the output power was calculated more accurately for the high power baseline case with hydrogen as working gas.

Sullivan (1989) also gave detail of a range of other measurements conducted at the NASA Lewis Research Centre. Figures 7 – 12 show several variables against engine speed for measurements conducted with helium as working fluid, with the average pressure close to 4.2 MPa and with the heater tube gas temperature close to 650 °C. (These are the same conditions as for the measured results shown in Table 2.) The graphs are presented to compare the ability of the numerical formulation to accurately predict the different variables as a function of engine speed.

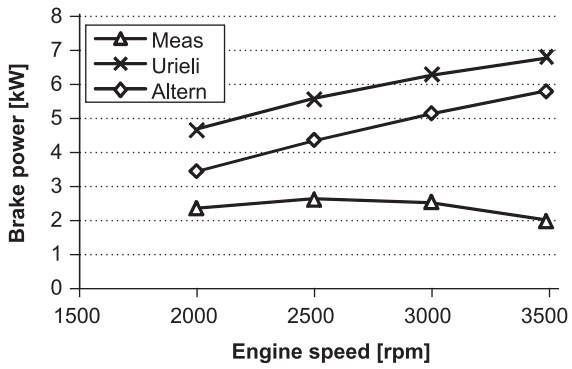


**Figure 7: Measured brake output power and simulated indicated output power**

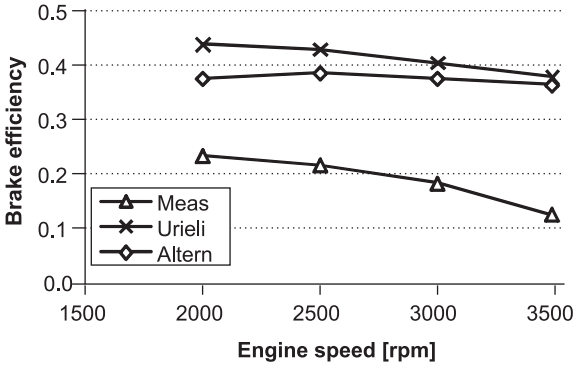


**Figure 8: Measured brake efficiency and simulated indicated efficiency**

Figures 7 and 8 show the measured brake output power and efficiency and simulated indicated output power and efficiency as a function of engine speed respectively. It follows therefore that the simulated output power and efficiency is predicted to be significantly higher than for the actual case for both the Urieli and alternative methods. In addition, while the measured output power starts to decrease with increasing engine speed, the simulated output power still increases at a decreasing rate for both methods. The simulated efficiency, however, shows more or less the same trend as for the measured case.

The pressure profiles obtained from simulation by Urieli (1977) using a third order formulation suggested that a simplified momentum equation could be used for simulation up to peak power. Urieli (1977) however, showed that even at engine speed well below that of peak power, a complete momentum equation including momentum flux and acceleration terms should be used. For helium, peak power is reached in the region of 2 500 to 3 000 rpm. From more or less this point and onwards, irregularities in the expansion space pressure profiles appear. Urieli (1977) found that a choking type local pressure peak appeared in his simulations using air as working fluid. This pressure peak impacted negatively on the output power. These phenomena can only be simulated with formulations far more complex than the second order formulation presented here, hence the inability of the simulated output power to follow the decreasing trend of the measured output power.

Figure 9 shows the measured heat input to the engine and simulated heat input to the gas against engine speed, while Figure 10 shows the measured and simulated heat output of the engine.

The heat input to the gas will be the larger part of, but will not exceed, the total heat input to the engine. The simulated heat input to the gas using the alternative method is therefore more accurate. The heat output as determined by the alternative method – again, is also more accurate.

Figure 11 shows the measured and simulated

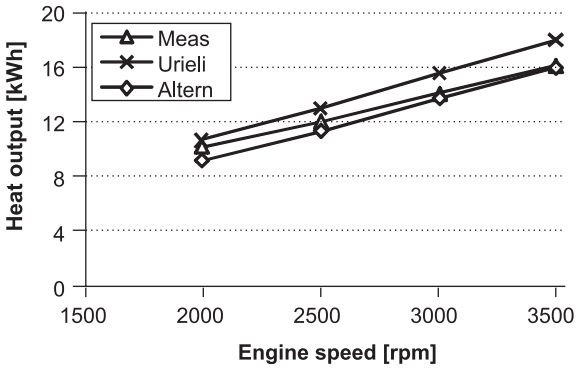


**Figure 9: Measured heat input to engine and simulated heat input to gas**

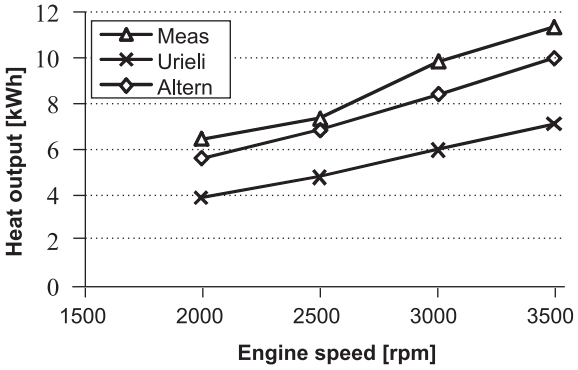


**Figure 10: Measured and simulated heat output**

expansion space pressure swing against engine speed and Figure 12 shows the measured and simulated compression space pressure swing against engine speed.

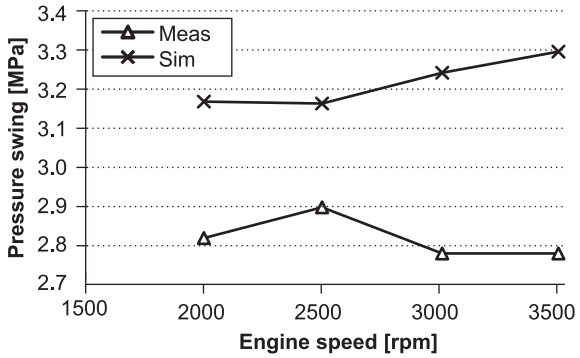


**Figure 11: Measured and simulated expansion space pressure swing**

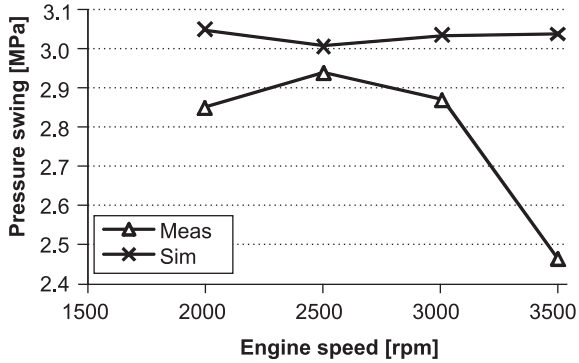


**Figure 12: Measured and simulated compression space pressure swing**

The simulated trends for the pressure swing against engine speed for both the expansion space and compression space do not follow those of the measured pressure swings. In the case of the expansion space, an increase in pressure swing is predicted, while the measured pressure swing shows a decrease as engine speed increases.

For the compression space, a sharply decreasing pressure swing was presented by Sullivan (1989) for increasing engine speed for measurements with average pressure at close the 4.2 MPa. However, the validity of the measured pressure swing at 3 500 rpm is questioned, because no other similar decreases were observed for measurements presented by Sullivan (1989) at average pressures of 2.8 MPa and 5.6 MPa. The pressure swing obtained from measurements at these average pressures stayed rather constant over the same range of engine speed. If it is indeed the case that the pressure swing was measured incorrectly at 3 500 rpm for the data shown in Figure 12, then the simulated pressure swing predicts the actual pressure swing more accurately than for the expansion space.

Figures 13 – 18 show several variables against engine speed for measurements conducted with hydrogen and helium as working fluid, with the average pressure close to 2.8 MPa and with the heater tube gas temperature close to 700 °C.

Figures 13 and 14 show the measured brake output power and efficiency and simulated indicated output power and efficiency as a function of engine speed respectively, similar to the data shown in Figures 7 and 8. The simulated output power and efficiency as predicted by the alternative method are shown to be more accurate for both hydrogen and helium, especially at a lower engine speed. At higher engine speed, it is shown that the simulations become less accurate for reasons already discussed previously.

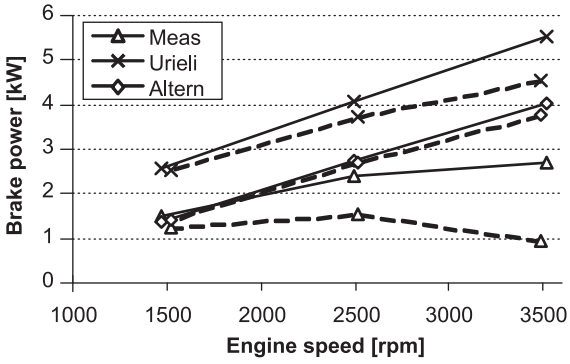


**Figure 13: Measured brake output power and simulated indicated output brake power for hydrogen (solid line) and helium (dashed line)**

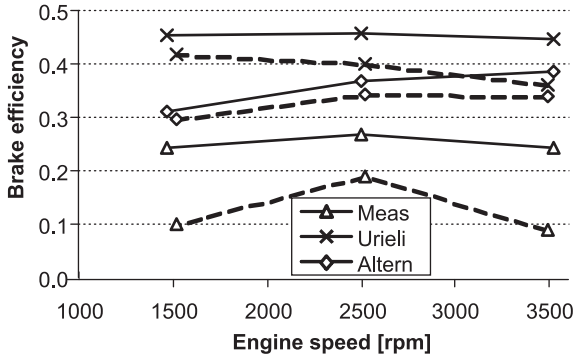


**Figure 14: Measured brake efficiency and simulated indicated efficiency for hydrogen (solid line) and helium (dashed line)**

Figure 15 shows the measured heat input to engine and simulated heat input to gas against engine speed, while Figure 16 shows the measured and simulated heat output of the engine. The data trends for both cases are very similar to the data shown in Figures 9 and 10 and the same comments given previously apply for the data shown in Figures 15 and 16.

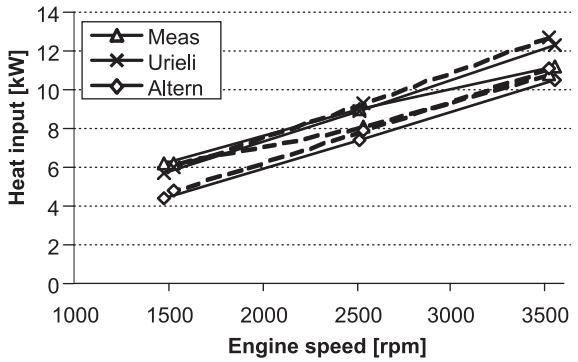


**Figure 15: Measured heat input to engine and simulated heat input to gas for hydrogen (solid line) and helium (dashed line)**

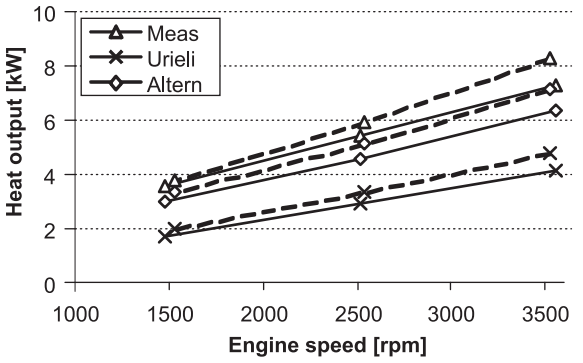


**Figure 16: Measured and simulated heat output for hydrogen (solid line) and helium (dashed line)**

Figures 17 and 18 show the measured and simulated expansion space and compression space pressure swing against engine speed respectively. The simulated trends for the pressure swing against engine speed for both the expansion space and compression space show limited success in following the trend of the measured pressure swings. Overall, the pressure swings are overestimated by the simulations by up to about 27 % and 20 % for the expansion space and compression space respectively.

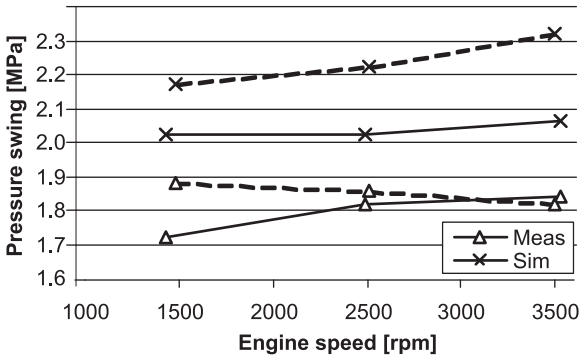


**Figure 17: Measured and simulated expansion space pressure swing for hydrogen (solid line) and helium (dashed line)**

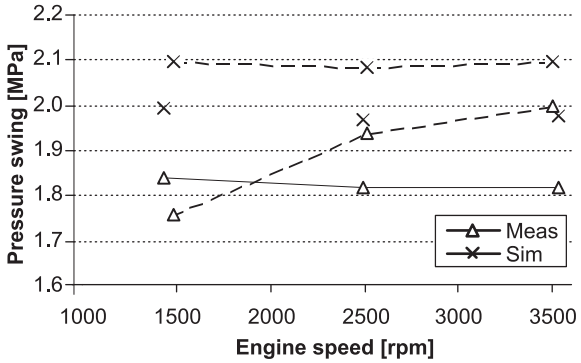


**Figure 18: Measured and simulated compression space pressure swing for hydrogen (solid line) and helium (dashed line)**

In general, the various operational variables were estimated fairly accurately in most cases or alternatively the measured trends were followed to a fair degree as a function of engine speed, especially with hydrogen as working fluid. Where discrepancies exist, the measured value is either in question or larger inaccuracies occur due to higher engine speed.

## 6. Conclusions

In this paper, implementation of a second order formulation for Stirling engine simulation as developed by Urieli (2001), with improvements and the verification of its simulation accuracy against the known performance of the GPU-3 Stirling engine, was reported. The objective of this investigation was to establish a simulation tool to perform preliminary engine design and optimisation.

The overall accuracy of the simulations with the exception of the output power and efficiency

proved to be satisfactory. The alternative method yielded more accurate results compared to the method used by Urieli in estimation of the various other operational variables. Where large inaccuracies occurred for some of the operational variables, the simulated trends in general followed the measurements.

The limitations of the second order formulation presented here, e.g. the inability to account for the interrelated nature of the loss mechanisms, were highlighted. Where more accurate simulation and more detailed information of the thermodynamic and gas dynamic behaviour are needed, a third order formulation would be more appropriate. No comparison is available that compares the processing time of third order formulations with second order formulations. Nevertheless, due to its simplified nature, the second order formulation presented here is considered more suitable as a first iteration design and optimisation tool.

## References


Berchowitz, D.M. (1978). *A* Computer and Experimental Simulation of Stirling Cycle Machines, M Sc dissertation, University of the Witwatersrand, Johannesburg.

Berchowitz, D.M. (1986). Stirling Cycle Engine Design and Optimisation, PhD dissertation, University of the Witwatersrand, Johannesburg.

Berchowitz, D.M. & Urieli, I. (1984). Stirling Cycle Machine Analysis, Adam Hilger.

Hargreaves, C. M. (1991). The Phillips Stirling Engine, Elsevier, Amsterdam.

Organ, A.J. (1992). Thermodynamics and Gas Dynamics of the Stirling Cycle Machine, Cambridge University Press, Cambridge.

Organ, A.J. (1997). The Regenerator and the Stirling Engine, Mechanical Engineering Publications Limited, London and Bury St. Edmunds.

Snyman, H., Harms, T.M. & Strauss, J.M. (2008). Design Analysis Methods for Stirling Engines, *Journal of Energy in Southern Africa*, Vol. 19, No. 3, Cape Town.

Sullivan, J.S. (1989). NASA Lewis Stirling Engine Computer Code Evaluation. Report DOE/NASA /4105-4 prepared for the U.S. Department of Energy, Office of Vehicle and Engine R&D, Washington DC.

Thieme, L.G. (1979). Low-power baseline test results for the GPU-3 Stirling engine. Report DOE/NASA/1040-79/6 prepared for U.S. Department of Energy, Office of Conservation and Solar Applications, Div. of Transportation Energy Conservation, Washington DC.

Thieme, L.G. (1981). High-power baseline and motoring test results for the GPU-3 Stirling engine. Report DOE/NASA/51040-31 prepared for U.S. Department of Energy, Office of Vehicle and Engine R&D, Washington DC.

Urieli, I. (1977). A Computer Simulation of Stirling Cycle Machines, PhD dissertation, University of the Witwatersrand, Johannesburg.

Urieli, I. (2001). Stirling Cycle Machine Analysis. URL: */www.ent.ohiou.edu/~urieli/stirling/me422.html.*


## Appendix A: Summary of the equation set for ideal adiabatic analysis

The equation set for the ideal adiabatic analysis as developed by Urieli (2001) is given below:

Equations for instantaneous pressure variation:

$$p = MR/\left(V_c/T_c + V_k/T_k + V_r/T_r + V_h/T_h + V_e/T_e\right)$$

$$dp = \frac{-\gamma p\left(dV_c/T_{ck} + dV_e/T_{he}\right)}{\left(V_c/T_{ck} + \gamma\left(V_k/T_k + V_r/T_r + V_h/T_h\right) + V_e/T_{he}\right)}$$

Equations for gas masses in each cell:

$$m_c = pV_c/\left(RT_c\right)$$

$$m_k = pV_k/\left(RT_k\right)$$

$$m_r = pV_r/\left(RT_r\right)$$

$$m_h = pV_h/\left(RT_h\right)$$

$$m_e = pV_e/\left(RT_e\right)$$

Equations for mass accumulation in each cell:

$$dm_c = \left(p\,dV_c + V_c\,dp/\gamma\right)/\left(RT_{ck}\right)$$

$$dm_e = \left(p\,dV_e + V_e\,dp/\gamma\right)/\left(RT_{he}\right)$$

$$dm_k = m_k\,dp/p$$

$$dm_r = m_r\,dp/p$$

$$dm_h = m_h\,dp/p$$

Equations for mass flow over cell interfaces:

$$m'_{ck} = -dm_c$$
$$m'_{kr} = m'_{ck} - dm_k$$
$$m'_{he} = -dm_e$$
$$m'_{rh} = m'_{he} - dm_h$$

Equations for conditional temperatures depending on the direction of flow:

$$\text{if } m'_{ck} > 0 \text{ then } T_{ck} = T_c \text{ else } T_{ck} = T_k$$
$$\text{if } m'_{he} > 0 \text{ then } T_{he} = T_h \text{ else } T_{he} = T_e$$

Equations for temperature change in the working spaces:

$$dT_c = T_c\left(dp/p + dV_c/V_c - dm_c/m_c\right)$$
$$dT_e = T_e\left(dp/p + dV_e/V_e - dm_e/m_e\right)$$

Equations for energy:

$$dQ_k = V_k\, dp\, c_v/R - c_p\left(T_{ck}\, m'_{ck} - T_{kr}\, m'_{kr}\right)$$
$$dQ_r = V_r\, dp\, c_v/R - c_p\left(T_{kr}\, m'_{kr} - T_{rh}\, m'_{rh}\right)$$
$$dQ_h = V_h\, dp\, c_v/R - c_p\left(T_{rh}\, m'_{rh} - T_{he}\, m'_{he}\right)$$
$$dW_c = p\, dV_c$$
$$dW_e = p\, dV_e$$
$$dW = dW_c + dW_e$$
$$W = W_c + W_e$$

## Appendix B: Specifications of the General Motors GPU-3 Stirling engine

***General***

| | |
|---|---|
| Configuration | Single-cylinder, uniform diameter bore. Rhombic drive crank mechanism |
| Working fluid(s) | He, $H_2$ |
| Rated maximum output | 8.95 kW with Hydrogen at 69 bar and 3600 rpm |
| Bore | 69.9 mm |
| Stroke (piston and displacer) | 31.2 mm |
| Working fluid circuit dimensions | |

***Heater***

| | |
|---|---|
| Mean tube length | 245.3 mm |
| Length exposed to heat source | 77.7 mm |
| Tube length(cylinder side) | 116.4 mm |
| Tube length (regenerator side) | 128.9 mm |
| Tube inside diameter | 3.02 mm |
| Tube outside diameter | 4.83 mm |
| No. complete tubes per cylinder | 40 |
| No. of tube per regenerator | 5 |

***Cooler***

| | |
|---|---|
| Tube length | 46.1 mm |
| Length exposed to coolant | 35.5 mm |
| Tube inside diameter | 1.08 mm |
| Tube outside diameter | 1.59 mm |
| No. of tubes per cylinder | 312 |
| No. of tubes per regenerator | 39 |

***Compression-end connecting ducts***

| | |
|---|---|
| Length | 15.9 mm |
| Duct inside diameter | 5.97 mm |
| No. of ducts per cylinder | 8 |
| Cooler end cap | 279 $mm^3$ |

***Regenerators***

| | |
|---|---|
| Housing inside length | 22.6 mm |
| Housing internal diameter | 22.6 mm |
| No. regenerators per cylinder | 8 |
| Mesh material | Stainless steel |
| Mesh no. | 7.9 wires/mm |
| Wire diameter | 0.04 mm |
| No. of layers | 308 |
| Porosity | 70% |
| Screen-to-screen rotation | 5° |

***Drive mechanism***

| | |
|---|---|
| Crank eccentricity, *r* | 13.8 mm |
| Connecting rod length, *l* | 46.0 mm |
| Désaxé offset, *e* | 20.8 mm |
| Linear expansion space clearance | 1.63 mm |
| Linear compression space clearance | 0.3 mm |
| Minimum working space volume | 232 350 $mm^3$ |

*Received 30 April 2009; revised 16 April 2010*